Research Article | Vol. 29, No. 22 / 25 Oct 2021 / Optics Express 35877
Optics EXPRESS

Analysis of laser plasma dynamics using the time resolved nonlinear optical response of ablated carbon nanocomposites mixed with epoxy resin

VYACHESLAV V. KIM,[1,2] RASHID A. GANEEV,[1,2,3,*] KONDA SRINIVASA RAO,[1] WEILI YU,[1] AND WEI LI[1]

[1]GPL, State Key Laboratory of Applied Optics, Changchun Institute of Optics, Fine Mechanics and Physics, Chinese Academy of Sciences, Changchun 130033, China
[2]Institute of Astronomy, University of Latvia, Riga LV–1586, Latvia
[3]Department of Physics, Voronezhy State University, Voronezh 394006, Russia
[*]rashid_ganeev@mail.ru

Abstract: Nonlinear optical properties of carbon nanostructures attract attention due to the unique response of these materials during interactions with ultrashort laser pulses. Here we probe the carbon nanocomposites mixed with epoxy resin in laser-induced plasmas using the high-order harmonics generation (HHG) method. We analyze the nanosecond pulses induced plasmas containing three carbon nanostructures (fullerenes, multiwalled carbon nanotubes and diamond nanoparticles) using 40 fs pulses propagating through these plasmas. HHG efficiencies in ablated graphite and nanocomposites are compared. We utilize two digitally synchronized (nanosecond and femtosecond) laser sources allowing for the HHG-based analysis of the evolution of different plasma plumes up to 10 μs delay from the beginning of ablation. The role of different carbon-containing nanocomposites is analyzed and the evidence for the presence of various nanomaterials in laser-induced plasma at the moment of propagation of the driving femtosecond pulses is demonstrated.

1. Introduction

High-order harmonic generation (HHG) in the laser-induced plasma (LIP) is a rich field for the studies of a variety of light-matter interactions, which attracted attention during last decade [1–25]. Any bulk material that undergoes ablation can be studied using a nonlinear optical method of harmonics generation. This opportunity gives possibilities in analysis of nanopowdered species by forming the composite targets in the shape of the pressed tablets consisting of various nanoparticles (NPs) or fixing the latter species in an adhesive matrix. Then these tablets or glued NPs can be ablated to form the plasma medium for HHG. The HHG of different inorganic NPs like metals and ferroelectric ceramics were studied in [26–28]. The comparison of the efficiency of harmonics generation in the plasmas produced during ablation of bulk targets and NPs of the same origin was presented in [29].

The carbon-contained targets demonstrated best properties as emitters of high-order harmonics [25,30–33]. The reason for this advantage has not yet been explained, although some similarities in the efficiency of HHG have also been experimentally demonstrated in the case of ablated bulk graphite as compared with bulk metal targets. In previous work [24], the role of different carbon-containing nanoparticles prepared in the form of the pressed tablets was investigated using two synchronized laser sources, one for laser ablation and second for HHG, providing a tunable delay between nanosecond heating pulse (HP) and femtosecond probing pulse (PP) in the range up to a few tens microseconds, in contrast to the most of previous studies where the delay between laser ablation of target and arrival of probing pulse did not exceed 100 ns.

#438075 https://doi.org/10.1364/OE.438075
Journal © 2021 Received 16 Jul 2021; revised 9 Sep 2021; accepted 17 Sep 2021; published 18 Oct 2021

Optics EXPRESS

The same approach is used in the current work. The application of longer delays is required to probe the plasma components moving at slow speeds. The delay between HP and PP in most of previous studies of HHG in LIPs is usually adjusted by the optical delay line. Taking into account the fact that the distance between the focus spot of femtosecond PP and target surface in those experiments usually did not exceed 150 - 300 μm, the analysis of plasma dynamics becomes restricted by consideration of the particles with minimum velocities at around 10^3 m/s. The presence of clusters and large NPs in LIPs requires the extension of delay between HP and PP in a much longer period than 100 ns. One can overcome this problem by using a separate laser for targets ablation, particularly, Nd: YAG laser providing 5 ns pulses. The use of longer (nanosecond) pulses for target ablation during HHG in LIP, as compared to picosecond pulses, has previously been analyzed in [34].

The dynamics of LIP spreading is quite complex since it involves the features of ablating material, laser–solid interactions, vapor/plasma formation, expansion, etc. The plume formed during laser ablation is also of considerable interest for plasma physics. Different methods could be used for LIP investigation, such as optical emission and absorption spectroscopy, time-of-flight mass spectrometry, imaging of plasma spreading, etc. The time-resolved methods for exploring LIP dynamics can be realized using laser-induced breakdown spectroscopy combined with the registration of plasma emission using the gated intensified charge-coupled device. The same type of detector can be used for time-resolved imaging of the spatial dynamics of LIP. Both these methods aim to analyze the plasma shape and emission at different delays between the ablation and registration. Notice that, due to rapid decrease of plasma density, excitation and emission, the efficiency of those methods is reducing at longer delays.

A few studies have been conducted to determine the optimal delays between HP and PP in the case of HHG using the plasmas containing similar main components, particularly, carbon atoms and carbon-containing NPs. In our research, three types of carbon NPs, fullerenes, multi-walled carbon nanotubes and diamond nanoparticles were used for preparation of composites with epoxy resin matrix. As reference samples, the ablated bulk graphite and pure epoxy were analyzed. In the present work, we also solve the main drawback of using the pressed tablets containing carbon nanoparticles - a fragility of targets preventing the optimal ablation of such targets followed by significant instability of the harmonic yield [24]. One way to resolve this issue is to fix the nanoparticles powder with epoxy matrix [35]. It is also known that carbon nanoparticles enhance the fracture strength, modulus, and yield strength of a polymer matrix [36]. Notably, carbon nanotubes (CNTs) possess advanced mechanical strength (Young′s modulus ~2 TPa) and elasticity, electrical strength and the ability to pass currents up to 10^{10} A/cm^2, high electron mobility and thermal conductivity. These features allow for the application of CNTs in various areas of science and technology.

In the present work, we have aimed at time-resolved exploration of LIPs evolution by probing the plasma using ultrashort, high intense femtosecond pulses resulting in HHG. We demonstrate that this method is effective for long delays (>1 μs) and for analysis of the slowly spreading heavy components of LIP. The unification of three above-described advanced approaches (i.e. use of carbon-based NPs in epoxy matrix, ablation of targets by additional laser source, and adjustment of delay between heating and probing pulses along a broad range) allows optimizing the conditions of HHG in the case of composite targets, as well as determining the role of different LIP components in harmonic generation. The results of these studies are useful for forming efficient sources of coherent extreme ultraviolet (XUV) radiation.

2. Experimental arrangements

Figure 1 shows the schematic view of the setup for LIP analysis via time-resolved HHG experiments. The main part of setup consists of two connected vacuum chambers with base pressure ~3×10^{-6} mbar. For laser plasma formation, the 5 ns heating pulses (λ=1064 nm, 10 Hz,

Optics EXPRESS

pulse energy up to 15 mJ) from Nd: YAG laser were focused inside the first chamber (VAC) on the surface of the targets by a 300 mm focal length spherical lens (FL1) providing the intensity up to ~2×10^9 W cm^{-2} and fluence up to ~12 J cm^2. In the XUV region, the time-integrated spectra of harmonics and plasma emission in the range of 10 to 100 nm were collected using the same XUV spectrometer as in [24]. For high-order harmonics generation, the femtosecond PP (40 fs, 800 nm, 1.5 mJ, 1 kHz) from femtosecond laser (Spitfire-Ace, Spectra-Physics) was focused inside the plasma plume by a 400 mm focal length spherical lens (FL2) providing the intensity of ~3×10^{14} W cm^{-2} inside the LIP at a distance of ~0.2 mm above the target surface. The intensity of PP inside the plasma plume was maintained at the same value for all samples. The harmonic emission was directed into the second chamber comprising the XUV spectrometer (XUVS), containing cylindrical mirror, flat-field grating and microchannel plate (MCP) for detecting the high harmonics. The HHG spectra were registered using the charge-coupled device (CCD) camera.

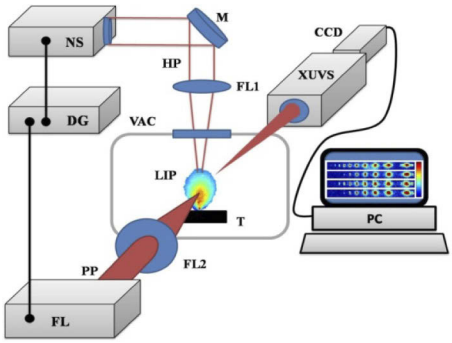

Fig. 1. Experimental setup for HHG and plasma dynamics studies. NS: nanosecond laser, FL: femtosecond laser, DG: delay generator, M: mirror, VAC: vacuum chamber, XUVS: extreme ultraviolet spectrometer, T: target, LIP: laser-induced plasma, F: fiber, FL1, FL2: focusing lenses for heating (HP) and probing (PP) pulses, CCD camera was connected with PC (personal computer) are used for registration of XUV spectra from the phosphor screen of MCP.

Digital synchronization of femtosecond and nanosecond lasers was performed using the digital delay generator (DG) DG535 (Stanford Research Systems). The delay between HP and PP at these conditions can vary from 0 to a few hundred microseconds.Whereas most of the experiments were carried out at the delays between 0 and 10 μs. The jitter between HP and PP in the plasma area was estimated to be ~15 ns.

Three materials were used for preparation of carbon-containing nanocomposites: C_{60} powder (C_{60}), multi-walled carbon nanotube powder (MWCNT, 15 nm width; the length of tubes was varied in the range of 500 nm – 20 μm) and diamond nanoparticles (DN, 20 nm size). These powdered materials were mixed with epoxy resin in weight ratio ~1:3, and the dried mixtures were formed as solid tablets. Along with nanocomposites, bulk graphite (Graphite) and pure epoxy resin (ER) without any additions were used in the experiments. All samples were purchased from Sigma-Aldrich.

3. Results

3.1. Characterization of LIP emission in XUV range

Here we present the time-integrated emission spectra of plasma radiation in the range of 30-100 nm (Fig. 2). The analysis of plasma emission lines in the XUV range provides information about different components in the plasma plume. In particular, we were able to determine the

Optics EXPRESS

presence of the particles at different ionization states and analyze the influence of nanoparticles on the formation of XUV emission. The emission lines were identified using NIST database [37].

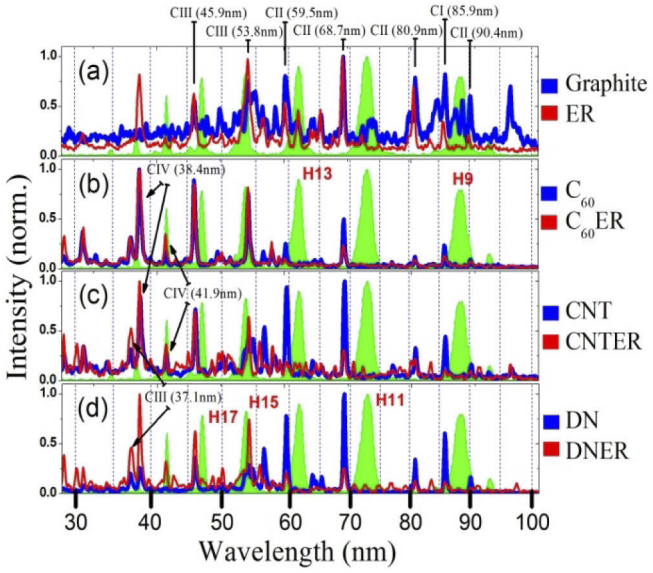

Fig. 2. Time-integrated XUV spectra from the ablated graphite, ER, pressed carbon nanostructures, and mixtures of different carbon-containing species and ER.

Heating pulses energies used at these experiments for recording plasma emission were same for different targets. We compared plasma emission from graphite, pure epoxy resin (ER), pressed tablets formed by pure powders of C_{60}, MWCNT (designated CNT in Fig. 2(c)) and DN, as well as the same powders in ER matrix. For the group of targets without ER the heating pulse energy was E_{HP}=6 mJ. In the case of pure ER, the pulse energy was highest (E_{HP}=15mJ) due to low absorption of heating laser radiation since pure ER tablet represents the partially transparent properties. For nanocomposites with three carbon-containing powders and ER, the heating pulse energy was kept equal to E_{HP}=9 mJ, which was 1.5 times higher than for solid graphite and pressed tablets but lower than for pure ER. In the case of pressed tablets, the heating pulse energies were limited due to the fragility of these samples. For example, in the case of DN pressed tablet, it was enough to shot few tens pulses to destroy this target. Notice that this problem was solved entirely in the case of the nanocomposites mixed with ER. We want to emphasize that all above-mentioned HP energies in the case of each target were a few times larger than those used for the optimal ablation allowing the achievement of the highest yield of harmonic emission. The optimal energy of HP for HHG corresponded to the formation of low-excited and low-ionized plasma when only harmonics, without or with weak plasma lines, were detected by XUV spectrometer.

The upper panel of Fig. 2 shows the emission spectra from ablated graphite (blue solid line) and epoxy resin (ER, red curve). On the background of all panels of Fig. 2 the filled green profiles show the positions of harmonics from the ninth order (H9) to H23, which are presented for comparison with the positions of strong emission lines of LIPs. Despite the fact, that ER is a compound comprising polymer material ($C_{21}H_{24}O_4$) and Si as a hardener component, the plasma emission did not demonstrate the presence of emission lines other than those attributed to the carbon ions (CI – CIV) in the studied spectral range (30–100 nm). Graphite spectrum lines (Fig. 2(a), blue curve) were appeared alongside with the continuum background. In the case of pure ER (red curve), the normalized intensity of the lines attributed to the low-charged carbon

Optics EXPRESS

ions and neutrals (CI and CII) was lower than in the case of emission from the graphite LIP, while CIV lines appeared in the spectrum of pure ER.

The subsequent panels (b), (c) and (d) of Fig. 2 show the emission lines for pairs of pure pressed (C_{60}, CNT, and DN, blue curves) retrieved at the experimental conditions similar to those analyzed in Ref. [24] and ER-fixed (red curves) carbon-based nanostructures (C_{60}ER, CNTER, and DNER). The common feature of those spectra is the better contrast of emission lines for all targets in comparison with bulk graphite and ER, as well as the increased contribution of higher-charged carbon ions. This behavior confirms the earlier reported observations pointing out the fact that, under similar experimental conditions, the plasma from carbon nanostructured materials could reach higher ionization states than the one in the case of bulk graphite ablation [38]. The emission from ER + nanocomposites containing LIPs (C_{60}ER, CNTER, DNER, Fig. 2) has similar pattern with strong lines for CIII and CIV transitions and suppressed lines in the spectral range between 60 and 100 nm. So the main effect of adding the ER matrix is related with the increase of the degree of ionization although heating pulse energy was lower (E_{HP} = 9 mJ) for nanocomposite targets in comparison with pure ER (E_{HP} = 15 mJ). We assume that the carbon nanostructures in the epoxy matrix play a role of absorption centers for laser radiation, thus efficiently increasing the energy coupling from the laser pulses.

3.2. HHG in graphite, pure epoxy and carbon-containing nanocomposites

In the case of HHG studies, PP was focused at a distance ~0.2 mm above the surface of ablating target. This means that, in principle, based on the estimates of plasma speed equal to ~10^4 m/sec, the fastest and least dense part of LIP reaches the axis of PP propagation at the timescale less than few tens nanosecond. Since the efficiency of generating harmonics depends on many factors, the "optimal" period from the ablation when densest part of plasma starts interacting with PP can be determined using delay-dependent HHG studies.

Below we present the comparative time-dependent studies of HHG in the graphite, pure epoxy and carbon-containing nanocomposites plasmas. HHG spectra were recorded at different delays between heating 5 ns pulses and driving 40 fs pulse using 100 ns steps of delay variation. For given targets, we compared harmonic spectra according to three points: analysis of harmonics distribution depending on the delay between HP and PP, determination of maximal HHG yield depending on the delay, and definition of the harmonic cutoff.

The summarized measurements are collected in Figs. 3 and 4 for HHG spectra at the delay range from 100 ns to 4 μs and the harmonic yield integrated in the range of 9^{th} to 27^{th} orders. The resulting intensity dependencies on delay are shown in Fig. 5(a).

Notice that the applied HP energies in the case of each sample varied in contrast to above-described incoherent XUV emission studies. The difference in HP energies for different samples is related to different "optimal conditions for plasma formation" to generate strong harmonics. For the convenience of presentation, the harmonic profiles for graphite and CNT in ER matrix (designated as CNTER) were grouped in Fig. 3 (black filled and blue filled profiles, correspondingly). The HHG data for epoxy resin, fullerenes and diamond nanoparticles in ER matrix are shown in Fig. 4 as red, green and blue profiles, respectively. Harmonics emission was recorded at the same conditions of registration for Figs. 3, 4 and 5. So despite the absence of absolute intensity measurements in the case of HHG, the relative values of harmonic emission for different targets could be compared using the scaling along the Y-axes in Figs. 3 and 4.

The optimal E_{HP} was highest in the case of HHG from pure ER (9 mJ) due to lower absorption of this material, while for other targets, and particularly for graphite, this value was in the range of ~3 mJ. ER is partially transparent for heating laser emission (λ=1064 nm), and for this reason, the harmonic yield in the case of lower energies of HP was extremely weak. For graphite (black filled curve and line in Figs. 3 and 5), the maximum delay at which we observed the weak harmonic emission was equal to 600 ns, while for ER and carbon-containing nanocomposites,

Optics EXPRESS

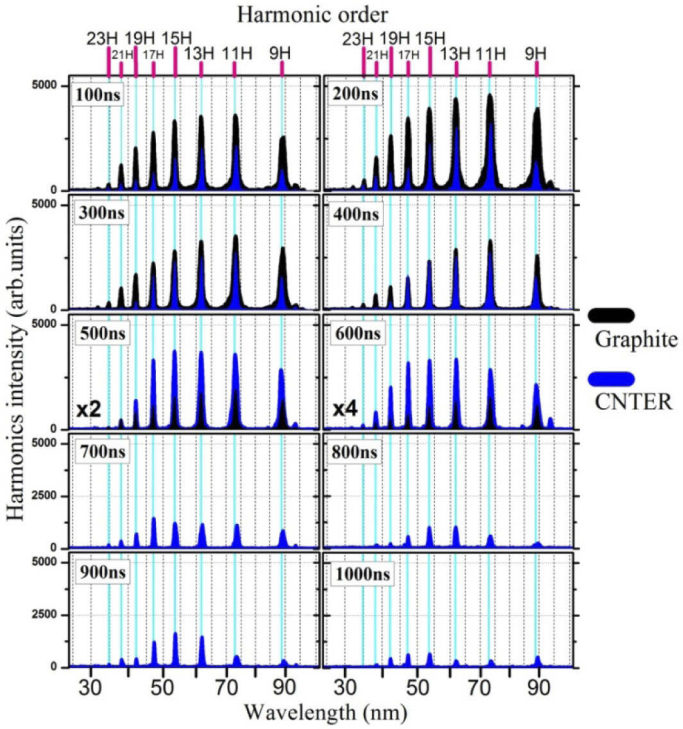

Fig. 3. Harmonic spectra obtained in the case of graphite (black filled profiles) and CNTER composite (blue filled profiles) LIPs at the delays varied between 100 ns and 1 μs. In the case of the panels for 500 and 600 ns delays, the harmonics from graphite are multiplied by the factors of 2× and 4× for better viewing.

the harmonics were observed at notably longer delays (up to 7 μs, not shown in the Figs. 3, 4 and 5 demonstrating HHG up the 4 μs delays). In the case of graphite (black line in Fig. 3), we determined the maximum of HHG at around 200 ns, while for ER the maximum of harmonic yield was shifted to ~1 μs and lasted up to 2 μs with further gradual decrease of HHG efficiency. Harmonics spectra from graphite in the delay range between 100 and 600 ns have a similar shape, with the plateau starting at 11^{th} order up to the 25^{th} order, which can be considered as the harmonic cutoff.

The envelopes of harmonic spectra from graphite plasma (Fig. 3, black filled profiles) were not changed for a whole studied delay range, with the harmonic intensity reaching the maximum at ~200 ns delay and gradually decreasing up to 600 ns delay. We attribute these dependencies by the presence of the same type of emitters within whole range of delay variations when a decrease of plasma density due to its expansion causes the decay in harmonic yield. According to the measured optimal delay (200 ns), the velocity associated with these emitters was estimated to be ~1×10^3 m/s taking into account the 0.2 mm distance between the target and the axis of PP propagation. This result is comparable with previously reported studies of the optimal delay for the third harmonic generation in carbon plasma (500 ns, when PPs were focused at a distance of 0.6 mm from target surface [39]).

The comparison of HHG in graphite and ER plasmas is important for further understanding the difference in HHG spectra from carbon nanostructures mixed with ER matrix. The patterns of harmonic spectra variations in the case of ER LIP are shown in Fig. 4 (red-filled profiles). One can distinguish three separate ranges of delays, at which HHG spectral shapes were varied

Optics EXPRESS

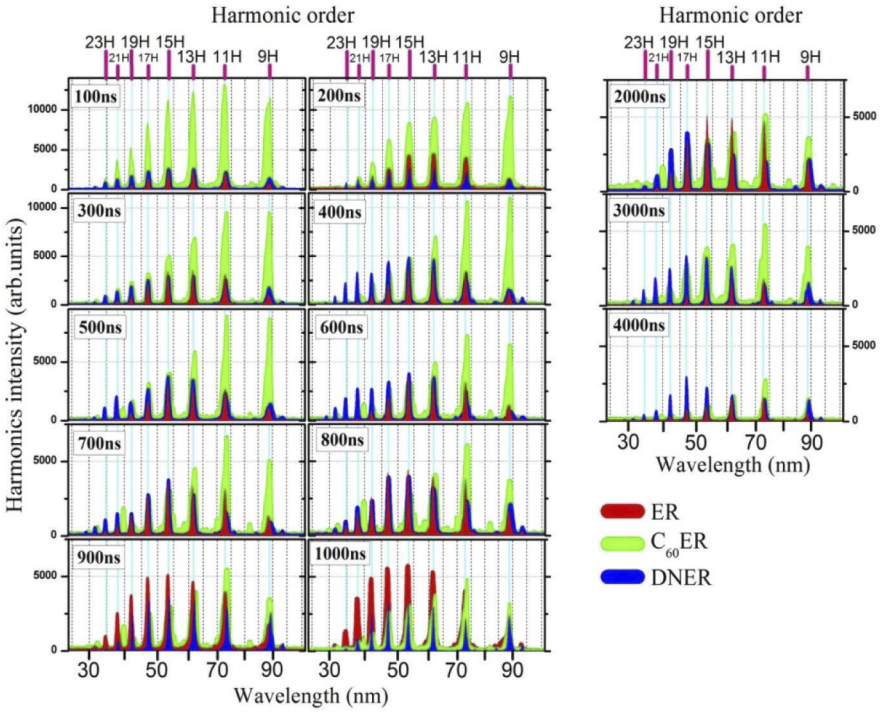

Fig. 4. Harmonic spectra in ER (red filled curves), DNER (blue filled curves) and C_{60}ER (green filled curves) LIPs at the delays varied between 100 ns and 4 μs.

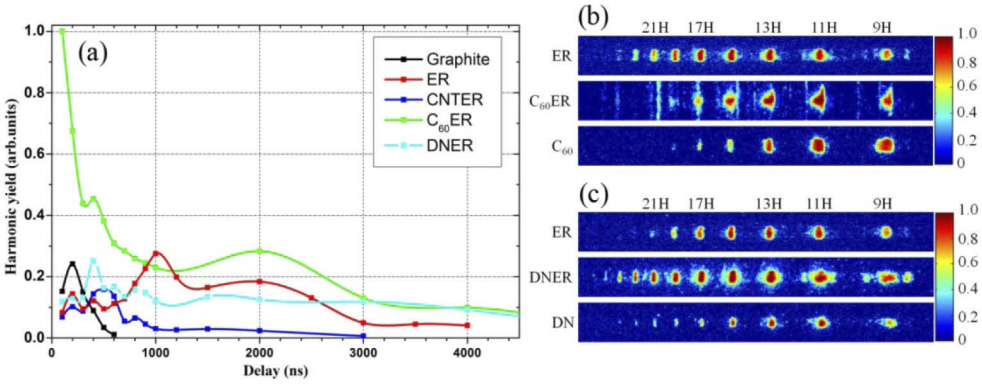

Fig. 5. (a) The delay dependencies of integrated harmonic yields from five LIPs. (b) Raw HHG spectra collected from ER, C_{60}ER and C_{60} LIPs at the delay equal 800 ns. (c) Raw HHG spectra collected from the ER, DNER and DN LIPs at the delay equal 400 ns.

Optics EXPRESS

by a different manner. At small delays (up to 300 ns), HHG spectra were similar to graphite. Starting from 400 ns delay, the dominant harmonic started shifting from 11^{th} to 17^{th} order and reached the maximum at around 1 μs from the beginning of ablation. At the same time, the cutoff harmonic also increased from 21^{th} to 25^{th} order. Finally, in the case of longer delays (2–4 μs), HHG spectra again demonstrated the dominance of the lower-order part of plateau harmonics.

Despite the fact that plasma emission from ER (Fig. 2) did not show the contribution of molecular components in XUV range, we associate such behavior of harmonic emission variations with the presence of the extended fragments of polymer chains in ER LIP. This assumption is supported by determining larger optimal delays andsmaller velocities (~2×10^2 m/s) for the emitters responsible for harmonics generation. HHG spectroscopy revealed much complex behavior for longer delays and confirmed the presence of low-speed components in ER LIP. There is a question how the harmonic spectra change in the case of composite targets with regard to the pure nanostructures and how to single out the role of nanostructures and ER in HHG while distinguishing the most attractive features of these mixed targets?

Below we address the above issues and analyze the harmonics generation from composite targets (multiwalled carbon nanotubes, C_{60} powders and diamond nanoparticles mixed with ER), while comparing with graphite and recognizing the contribution from ER. Figures 3 and 4 show the dependencies of harmonic yield at different delays between HP and PP in the case of ablated C_{60}ER (Fig. 4, green filled profiles), DNER (Fig. 4, blue filled profiles) and CNTER (Fig. 3, blue filled profiles). These composite targets were prepared at the ER:C_{60}, ER:DN and ER:CNT weight ratios of 3:1. At these conditions, the composites' ablation thresholds were strongly reduced compared to pure ER, while still being higher compared with the graphite. The corresponding optimal HP energies were ~6 mJ in the case of nanocomposite targets.

The plasma produced on the mixture of fullerene with ER and diamond nanoparticles with ER dramatically extended the delay range at which the harmonics can be observed (Fig. 5(a), green and cyan curves), as well as the cut-off position, especially in case of C_{60}ER, in comparison with the pure C_{60} [24]. This observation is also valid for the CNTER target but in lesser delays (Fig. 5(a), blue curve). The delay dependence for ablated C_{60}ER mixture demonstrated higher integrated harmonics yield and the extended range of delays between HP and PP at which the harmonics can be observed. The comparison of HHG spectra produced from ablated C_{60}ER mixture (Fig. 4, green filled curves) and other targets allows concluding that C_{60} molecules can be considered as most efficient emitters of high-order harmonics compared with other studied carbon-containing LIPs. Their presence in LIP leads to stronger enhancement of the low-order part of HHG spectrum comprising the harmonics between 9^{th} and 17^{th} orders. Despite the lower density of C_{60} in plasma compared with C atoms and ions originated from graphite ablation, higher HHG efficiency allows the observation of harmonics from fullerenes even at notably longer delays (more than 4000 ns) compared with the latter species.

In the case of C_{60}ER, one can see the mutual effect of each material. C_{60}ER mixture led to extension of the delay between pulses at which harmonics can be observed. At long delays and stronger laser ablation, the harmonics appear alongside with weak plasma emission (Fig. 4, panels between 700 and 2000ns delays). The second peculiarity of C_{60}ER plasma is the extended plateau and cutoff up to the 25^{th} order. Additionally, strong enhancement of the low-order part of HHG spectrum was observed, while the harmonics between 9^{th} and 17^{th} orders were generated for notably longer delays. These two effects can be attributed to the coherent contribution from ER leading to the extension of delays at which HHG emission could be observed and from C_{60} leading to the enhancement of a selected part of HHG spectrum. This observation proves the presence of C_{60} particles possessing a broad range of spreading velocities (from ~10^2 to ~10^3 m/s). The contribution of C_{60} to HHG spectra at specific delays can be also identified by analysis of HHG characteristic pattern as it demonstrated in panel (b) of Fig. 5, where the raw images normalized to 1 for ER and C_{60}ER at the 800 ns delay are compared with the raw spectra from

Optics EXPRESS

pure C_{60} pressed tablet (C_{60} panel in Fig. 5(b)) collected at the same experimental conditions as in [24]. The similarity of C_{60} and C_{60}ER harmonics spectra are obvious, with some presence of additional plasma emission lines in the case of C_{60}ER composite.

In the case of CNTER we also observed the extension of delay up to 3μs (Fig. 5(a), blue curve), but in contrast to C_{60}ER the presence of carbon nanotubes did not lead to enhancement of harmonics. HHG spectral pattern in that case, was similar to the one obtained from the graphite LIP with same cutoff. The only difference was a maximum harmonic yield shift towards the longer delays (~400 ns). We assume that CNT structures enforced the epoxy resin matrix and increased the relative fraction of carbon in ablated material, thus resulting in graphite-like HHG spectra with some already mentioned peculiarities.

An interesting peculiarity was observed in the case of harmonics generation from DNER composite. Again, as a common feature of ER mixed carbon nanocomposites, we observed the notable extension of delay at which HHG was observed (beyond 5 μs, Fig. 5(a), cyan line) with maximum yield at around 400 ns. Also we mention the slowly declining slope of integrated harmonic yield curve for the delays >1μs. Meantime, the analysis of delay-dependent HHG demonstrated quite different influence of diamond nanoparticles on the characteristic pattern of harmonics distribution. We observed the relative enhancement of the group of harmonics close to the cutoff region (Fig. 4, 400-800 ns panels, blue filled profiles) but without enhancing the overall harmonic yield, as it was demonstrated in the case of C_{60}ER LIP. Similar pattern we observed in the case of HHG in pure ER at around the "optimal" delay for this target (Fig. 4, 800-1000 ns panels, red filled profiles). The comparison of these results with HHG from pure DN target (Fig. 5(c), DN panel; the spectrum obtained at the same conditions as in [24]), showed, as it has been also demonstrated in [24], the diamond nanoparticles cannot be considered as the efficient emitters of harmonics among other carbon-containing nanostructures. One can conclude that DN in ER are playing a role of absorption centers for HP.

4. Discussion

The most important novelty of the present study is the analysis of the role of some accompanying species during frequency conversion of ultrashort lasers in the plasmas containing most perspective material (carbon NPs), allowing largest harmonic yield in the longer-wavelength region of extreme ultraviolet compared with other HHG approaches in gases and solids. This issue was not considered in Ref. [24]. Meanwhile, different components of laser-induced plasma can drastically change the harmonic spectrum and even the enhancement of conversion efficiency towards the shorter wavelength region. Our delay-dependent approach allows distinguishing the prevailing role of carbon-based nanostructures over the carbon-containing molecular systems used to maintain the former species during ablation and evaporation.

To carry out these studies we modified the method of targets formation. The particular difference between these two studies is the samples preparation. In [24], the pressed tablets of carbon nano-objects such as fullerenes, nanotubes, and diamond nanoparticles were studied. In present paper, we describe how the nanocomposite materials containing the above-mentioned carbon nano-objects embedded in the epoxy-resin matrix drastically change the dynamics of spreading out from the ablated surface. This change in plasma dynamics modifies the harmonics spectra depending on the moment of registration. Along a whole period of plasma formation, spreading, and decay, we determined and distinguished the role of the matrix, which has been proved to be a better approach in maintenance of carbon nanoparticles during longer period of targets ablation compared with the pure samples combined by pressing of the powders. Thus in present work, we solved the main drawback of using the pressed tablets containing carbon nanoparticles - a fragility of targets preventing the optimal ablation of such targets followed by significant instability of the harmonic yield.

Optics EXPRESS

The role of the pulse width during plasma formation is a crucial parameter during consideration of the ablation mechanism, which was underlined in a few previous studies, particularly in the case of the harmonics generation in the laser-induced plasmas ignited by nano-, pico-, and femtosecond pulses [34]. Once considering this particular process (HHG in plasma), the advanced features of picosecond and femtosecond ablation compared with ablation by nanosecond pulses were confirmed in various studies. Meanwhile, the former lasers cannot provide the opportunity in determination of the influence of plasma dynamics on the harmonics spectra and cut-offs, whilst nanosecond lasers being separately synchronized with femtosecond driving sources allow the analysis of ablation plume through the delay-dependent studies of harmonic spectra variations along the extended (1–10^6 ns) timescale from the beginning of ablation. This feature was a motivation in choosing the configuration of the fs + ns laser for our experiments.

The important parameter that has rarely been explored during plasma HHG studies is heating pulse duration. The absorbance of long pulses notably differs from the one using the shorter-duration heating emission. Since almost all of the HHG studies from plasma plumes were carried out by using the heating pulses of a few hundred picosecond pulse duration, the conclusion was drawn about the optimal intensity of the pulse radiation at the target surface (~(1–4)×10^{10} W cm^{-2}), depending on the absorptive properties of ablated material [40]. It is interesting to compare the HHG from the plasmas, especially those used in present experiments, produced by the pulses of different duration since it can clarify which parameter (energy, fluence, or intensity) of the heating radiation plays a crucial role in the formation of optimal plasma.

The observed behavior of the harmonics variation during our experiments can be attributed to the dynamic characteristics of the plasmas in the cases of the low- and high-Z target materials. Light particles possess higher velocity and this can lead to the depletion of the concentration of the particles in the laser-plasma after a few tens of nanoseconds. At the same time, the high- and medium-Z particles for a longer time remain close to the target surface where the HHG occurs. For heavy targets, the dependence of the high harmonic yield on the delay between the pulses is not so pronounced compared to the low-Z materials. The difference between these dependencies was clearly seen in our studies in the case of longer delays due to different concentration of the particles in the interaction area of a laser plume for the lower- and higher-Z targets. Based on this, the search of the optimal plasma conditions should take into account the role of the atomic characteristics of the targets.

Laser ablation of carbon-containing species has been intensively examined during the last ten years to define plasma conditions for the synthesis of carbon structures with unique properties, in particular, fullerenes and carbon nanotubes. The physical characteristics of the plasma plume, such as concentration of atoms and clusters, directly affect the properties of the material being formed in the dynamic expansion of the ablated material. Thus, to select the optimal plasma conditions for HHG, a detailed understanding of the basic physical processes governing the ablation plume composition and reliable methods for controlling the plume species are needed. This can be done using the ns + fs lasers configuration.

The use of nanosecond Nd: YAG lasers as the sources of heating pulses may also offer some additional advantages compared with the commonly used picosecond pulses of the same repetition rate and wavelength as the driving sources. The application of nanosecond pulses to ablate the surface of targets allows the formation of less-ionized and less-excited plasma during longer periods of laser-matter interaction compared with picosecond pulses. This conclusion is based on the analysis of the nanosecond and picosecond ablation-induced plasma emission in the visible and extreme ultraviolet ranges in the case of the formation of the optimal plasmas leading to the generation of the highest harmonic yields.

Meanwhile, ablation by nanosecond laser pulses most probably would lead to some disintegration of large nanostructures due to avalanche ionization and Joule heating, leading to the presence of both NPs and single molecular species in the plasma plume. It is not clear if HHG

Optics EXPRESS

solely happens from neutral and ionized NPs and nanoparticles/clusters generated due to ablation or it happens in charged species and ions. The electron density of such plasmas has never been measured.

Our observations give a rough pattern of the ablation by nanosecond pulses and HHG from carbon NP targets. The material around the NPs is a dried polymer (epoxy resin), which has a lower ablation threshold than carbon nanostructures. Therefore, the epoxy resin starts to ablate at relatively low intensities, carrying NPs with it, resulting in the lower heating pulse intensity required for the ablation and evaporation of the target resulting in clusters formation in the plasma volume.

The uncertainty of the exact mechanism of HHG from clusters has been outlined in a few early studies. Among the considered channels, ionization and recombination to the same atom, to the neighboring ions, and the whole nanoparticle have been proposed. In particular, it was suggested that HHG in Kr clusters is attributed to a mechanism in which delocalized electrons tunnel from a cluster and recollide coherently with the whole cluster. Notice that the experiments with gas clusters have revealed difficulty in disentangling the harmonics produced by different species (monomers and clusters of different sizes). In the meantime, the comparative studies of HHG in plasmas constituted by clusters and monomers show that, at equal experimental conditions, the latter emitters provide considerably weaker harmonic yield, thus pointing to the specific advanced properties of the clustered emitters of harmonics in the nanoparticle-containing plasmas.

As mentioned earlier, we tried to keep the concentration of carbon NPs high enough by using the 3:1 mass ratio of epoxy resin and nanoparticles. At these conditions, ER + powder compound became "black" and nontransparent, which allowed expecting excellent absorption of the heating pulses. As we noticed, the composites' ablation thresholds were strongly reduced compared to pure ER, while still being higher compared with the graphite. The optical properties of mixed materials for ablation can hardly be retrieved in the case of the used species. All of them, being mixed with epoxy resin, represent the black jelly prior to drying. They demonstrate good absorption of the 1064 nm nanosecond radiation. Probably, the insignificant difference in absorption of these nanosecond pulses should not play a crucial role in distinction of the heat transfer from the ablating photons to the carbon nanostructures.

Below we briefly address the elemental state of ablated species. We believe that mass-spectrometric experiments in the case of such complex targets deserve separate full-scale research. Notice that there are a few serious experimental difficulties in simultaneously determining the composition of plasma plumes using time-of-flight mass-spectrometric (ToFMS) studies and carrying out the HHG experiments. It is difficult to combine these two facilities in a single set of experiments. Notice also a difference in the experimental conditions for the formation of plasma for these two facilities. The ToFMS experiments can be performed separately from the HHG measurements; however, it is difficult to maintain absolutely identical ablation experiments in two setups taking into account a difference in the optimal fluencies of the heating laser pulses in these two cases.

The attempts to analyze the carbon-containing plasma were reported in the past [41]. In those studies, scanning electron microscopy (SEM) for the debris analysis and TOFMS of plasma characterization were defined separately from the HHG experiments. These two methods have provided useful clues about the conditions and dynamics of plasma plume formed above the carbon target surface. Whilst the former method can provide information about the presence of nanoparticles in the plasma, one has to cautiously consider those results from the following point of view. The deposition process on the substrate happens much later than the time of HHG emission, and the physical process of deposition may lead to further aggregation. Since SEM is an *ex-situ* method, one cannot exclude the difference between the real composition of clusters in the plasma and the results of SEM measurements, although it clearly proves the presence of multi-particle species in the plasma. TOFMS yields information on the *in situ* presence of

Optics EXPRESS

ionized clusters, although it requires ablation of the target under the same conditions as in the case of HHG experiments and is not well suited for the detection of neutral nanoparticles in the ablated plasma.

5. Conclusions

In conclusion, we presented the studies of the laser-induced plasmas during ablation of five carbon-containing materials (graphite, pure epoxy resin, fullerenes, multiwalled nanotubes and diamond nanoparticles in the matrix of epoxy resin). The methods of XUV spectroscopy and time-resolved nonlinear optical probing via HHG at different moments of LIPs evolution were used. The contribution of different plasma components from carbon nanostructure-containing targets in the range of 100 ns to 10 μs delays between HP and PP was analyzed using HHG. We have demonstrated the difference of the delay dependencies of harmonic yields from the plasmas produced on the bulk graphite and other nanoparticle-containing samples. A significant difference in the optimal delays for those species is determined. In the case of C_{60}ER, the analysis of delay dependencies of integrated harmonic yields and HHG spectra in the 30–100 nm wavelength range allowed determining the presence of C_{60} nanoparticles along the wide range of velocities (from $\sim 10^2$ to $\sim 10^3$ m/s). We have demonstrated that the presence of C_{60} nanoparticles leads to generation of enhanced harmonics in the wavelength range of 50–95 nm (i.e., of the harmonics from 9^{th} to 17^{th} orders). The difference in HHG arising from mixing of multiwalled nanotubes and diamond nanoparticles in epoxy matrix has been demonstrated and discussed. The key role of utilizing two digitally controlled laser sources for obtaining extensive delays between heating and probing pulses, in comparison with traditional optical delay scheme, was demonstrated. The presented studies allow for a better understanding of the role of plasma spreading dynamics in the harmonics generation from ablated species comprising the similar basic element (carbon) in form of nanocomposites.

Funding. Chinese Academy of Sciences President's International Fellowship Initiative (2021PM0036); European Regional Development Fund (1.1.1.5/19/A/003); State Assignment to Higher Educational Institutions of Russian Federation (FZGU-2020-0035).

Disclosures. The authors declare no conflicts of interest.

Data availability. Data underlying the results presented in this paper are not publicly available at this time but may be obtained from the authors upon reasonable request.

References

1. R. A. Ganeev, M. Suzuki, M. Baba, and H. Kuroda, "Harmonic generation from chromium plasma," Appl. Phys. Lett. **86**(13), 131116 (2005).
2. T. Ozaki, L. B. Elouga Bom, R. Ganeev, J.-C. Kieffer, M. Suzuki, and H. Kuroda, "Intense harmonic generation from silver ablation," Laser Part. Beams **25**(2), 321–325 (2007).
3. L.-B. Elouga Bom, F. Bouzid, F. Vidal, J.-C. Kieffer, and T. Ozaki, "Correlation of plasma ion densities and phase matching with the intensities of strong single high-order harmonics," J. Phys. B **41**(21), 215401 (2008).
4. R. A. Ganeev, L. B. Elouga Bom, M. C. H. Wong, J.-P. Brichta, V. R. Bhardwaj, P. V. Redkin, and T. Ozaki, "High-order harmonic generation from C_{60}-rich plasma," Phys. Rev. A **80**(4), 043808 (2009).
5. H. Singhal, V. Arora, B. S. Rao, P. A. Naik, U. Chakravarty, R. A. Khan, and P. D. Gupta, "Dependence of high-order harmonic intensity on the length of preformed plasma plumes," Phys. Rev. A **79**(2), 023807 (2009).
6. T. Ozaki, L. B. Elouga Bom, J. Abdul-Haji, and R. A. Ganeev, "Evidence of strong contribution from neutral atoms in intense harmonic generation from nanoparticles," Laser Part. Beams **28**(1), 69–74 (2010).
7. Y. Pertot, L. B. Elouga Bom, V. R. Bhardwaj, and T. Ozaki, "Pencil lead plasma for generating multimicrojoule high-order harmonics with a broad spectrum," Appl. Phys. Lett. **98**(10), 101104 (2011).
8. H. Sheinfux, Z. Hems, M. Levin, and A. Zigler, "Plasma structures for quasiphase matched high harmonic generation," Appl. Phys. Lett. **98**(14), 141110 (2011).
9. L. B. Elouga Bom, Y. Pertot, V. R. Bhardwaj, and T. Ozaki, "Multi-μJ coherent extreme ultraviolet source generated from carbon using the plasma harmonic method," Opt. Express **19**(4), 3677 (2011).
10. C. Hutchison, R. A. Ganeev, T. Witting, F. Frank, W. A. Okell, J. W. G. Tisch, and J. P. Marangos, "Stable generation of high-order harmonics of femtosecond laser radiation from laser produced plasma plumes at 1 kHz pulse repetition rate," Opt. Lett. **37**(11), 2064 (2012).

Optics EXPRESS

11. S. Haessler, L. B. Elouga Bom, O. Gobert, J.-F. Hergott, F. Lepetit, M. Perdrix, B. Carré, T. Ozaki, and P. Salières, "Femtosecond envelope of the high-harmonic emission from ablation plasmas," J. Phys. B **45**(7), 074012 (2012).
12. M. Kumar, H. Singhal, J. A. Chakera, P. A. Naik, R. A. Khan, and P. D. Gupta, "Study of the spatial coherence of high order harmonic radiation generated from pre-formed plasma plumes," J. Appl. Phys. **114**(3), 033112 (2013).
13. S. Haessler, V. Strelkov, L. B. Elouga Bom, M. Khokhlova, O. Gobert, J.-F. Hergott, F. Lepetit, M. Perdrix, T. Ozaki, and P. Salières, "Phase distortions of attosecond pulses produced by resonance-enhanced high harmonic generation," New J. Phys. **15**, 013051 (2013).
14. H. Singhal, P. A. Naik, M. Kumar, J. A. Chakera, and P. D. Gupta, "Enhanced coherent extreme ultraviolet emission through high order harmonic generation from plasma plumes containing nanoparticles," J. Appl. Phys. **115**(3), 033104 (2014).
15. R. A. Ganeev, M. Suzuki, and H. Kuroda, "Quasi-phase-matching of high-order harmonics in multiple plasma jets," Phys. Rev. A **89**(3), 033821 (2014).
16. N. Rosenthal and G. Marcus, "Discriminating between the role of phase matching and that of the single-atom response in resonance plasma-plume high-order harmonic generation," Phys. Rev. Lett. **115**(13), 133901 (2015).
17. M. A. Fareed, V. V. Strelkov, N. Thiré, S. Mondal, B. E. Schmidt, F. Légaré, and T. Ozaki, "High-order harmonic generation from the dressed autoionizing states," Nat Commun **8**(1), 16061 (2017).
18. M. Wöstmann, L. Splitthoff, and H. Zacharias, "Control of quasi-phase-matching of high-harmonics in a spatially structured plasma," Opt. Express **26**(11), 14524 (2018).
19. Z. Abdelrahman, M. A. Khohlova, D. J. Walke, T. Witting, A. Zair, V. V. Strelkov, J. P. Marangos, and J. W. G. Tisch, "Chirp-control of resonant high-order harmonic generation in indium ablation plumes driven by intense few-cycle laser pulses," Opt. Express **26**(12), 15745 (2018).
20. M. A. Fareed, V. V. Strelkov, M. Singh, N. Thiré, S. Mondal, B. E. Schmidt, F. Légaré, and T. Ozaki, "Harmonic generation from neutral manganese atoms in the vicinity of the giant autoionization resonance," Phys. Rev. Lett. **121**(2), 023201 (2018).
21. M. Kumar, H. Singhal, and J. A. Chakera, "High order harmonic radiation source for multicolor extreme ultraviolet radiography of carbon plumes," J. Appl. Phys. **125**(15), 155902 (2019).
22. M. Singh, M. A. Fareed, A. Laramée, E. Isgandarov, and T. Ozaki, "Intense vortex high-order harmonics generated from laser-ablated plume," Appl. Phys. Lett. **115**(23), 231105 (2019).
23. J. Liang, Y. H. Lai, W. Fu, Y. Shan, W. Yu, and C. Guo, "Observation of resonance-enhanced high-order harmonics from direct excitation of metal nanoparticles with femtosecond pulses," Phys. Rev. A **102**(5), 053117 (2020).
24. R. A. Ganeev, V. V. Kim, K. S. Rao, and C. Guo, "Probing laser plasma dynamics using high-order harmonics generation in carbon-containing nanomaterials," Appl. Sci. **11**(5), 2143 (2021).
25. V. V. Kim, R. A. Ganeev, G. S. Boltaev, M. Iqbal, and A. S. Alnaser, "Carbon nanostructure containing plasma: Medium for efficient high-order harmonics of 1030 nm laser," Phys. Plasmas **28**(2), 023111 (2021).
26. R. A. Ganeev, C. Hutchison, M. Castillejo, I. Lopez-Quintas, F. McGrath, D. Y. Lei, and J. P. Marangos, "Ablation of nanoparticles and efficient harmonic generation using a 1-kHz laser," Phys. Rev. A **88**(3), 033803 (2013).
27. H. Singhal, R. A. Ganeev, P. A. Naik, A. K. Srivastava, A. Singh, R. Chari, R. A. Khan, J. A. Chakera, and P. D. Gupta, "Study of high-order harmonic generation from nanoparticles," J. Phys. B **43**(2), 025603 (2010).
28. R. A. Ganeev, G. S. Boltaev, V. V. Kim, and C. Guo, "Effects of laser plasma formation on quasi-phase matching of high-order harmonics from nanoparticles and atoms," Nanomaterials **9**(4), 572 (2019).
29. H. Singhal, R. A. Ganeev, P. A. Naik, J. A. Chakera, U. Chakravarty, H. S. Vora, A. K. Srivastava, C. Mukherjee, C. P. Navathe, S. K. Deb, and P. D. Gupta, "High-order harmonic generation in a plasma plume of *in situ* laser-produced silver nanoparticles," Phys. Rev. A **82**(4), 043821 (2010).
30. R. A. Ganeev, P. A. Naik, H. Singhal, J. A. Chakera, M. Kumar, M. P. Joshi, A. K. Srivastava, and P. D. Gupta, "High-order harmonic generation in carbon-nanotube-containing plasma plumes," Phys. Rev. A **83**(1), 013820 (2011).
31. R. A. Ganeev, P. A. Naik, H. Singhal, J. A. Chakera, M. Kumar, U. Chakravarty, and P. D. Gupta, "Use of carbon-containing materials for efficient high-order harmonic generation of laser radiation," Opt. Commun. **285**(12), 2934–2941 (2012).
32. R. A. Ganeev, T. Witting, C. Hutchison, F. Frank, P. V. Redkin, W. A. Okell, D. Y. Lei, T. Roschuk, S. A. Maier, J. P. Marangos, and J. W. G. Tisch, "Enhanced high-order-harmonic generation in a carbon ablation plume," Phys. Rev. A **85**(1), 015807 (2012).
33. R. A. Ganeev, M. Baba, M. Suzuki, and H. Kuroda, "Morphology of laser-produced carbon nanoparticle plasmas and high-order harmonic generation of ultrashort pulses in clustered media," J. Phys. B **47**(13), 135401 (2014).
34. R. A. Ganeev, M. Suzuki, M. Baba, and H. Kuroda, "High-order harmonic generation from laser plasma produced by pulses of different duration," Phys. Rev. A **76**(2), 023805 (2007).
35. R.F. Gibson, "A review of recent research on mechanics of multifunctional composite materials and structures," Composite Structures **92**(12), 2793–2810 (2010).
36. F. F. Komarov, O. V. Milchanin, I. D. Parfimovich, M. V. Grinchenko, I. N. Parhomenko, A. G. Tkachev, and D. S. Bychanok, "Absorption and reflectance spectra of microwave radiation by an epoxy resin composite with multi-walled carbon nanotubes," J. Appl. Spectrosc. **84**(4), 596–602 (2017).
37. A. Kramida, Yu. Ralchenko, J. Reader, and and NIST ASD Team (2021). NIST Atomic Spectra Database (ver. 5.1). Available: http://physics.nist.gov/asd National Institute of Standards and Technology, Gaithersburg, MD.

Optics EXPRESS

38. C. Wülker, W. Theobald, D. Ouw, F. P. Schäfer, and B. N. Chichkov, "Short-pulse laser-produced plasma from C_{60} molecules," Opt. Commun. **112**(1-2), 21–28 (1994).
39. I. Lopez-Quintas, M. Oujja, M. Sanz, M. Martín, R.A. Ganeev, and M. Castillejo, "Low-order harmonic generation in nanosecond laser ablation plasmas of carbon containing materials," Appl. Surf. Sci. **278**, 33–37 (2013).
40. L. B. Elouga Bom, J.-C. Kieffer, R. A. Ganeev, M. Suzuki, H. Kuroda, and T. Ozaki, "Influence of the main pulse and prepulse intensity on high-order harmonic generation in silver plasma ablation," Phys. Rev. A **75**(3), 033804 (2007).
41. R. A. Ganeev, C. Hutchison, T. Witting, F. Frank, W. A. Okell, A. Zaïr, S. Weber, P. V. Redkin, D. Y. Lei, T. Roschuk, S. A. Maier, I. López-Quintás, M. Martín, M. Castillejo, J. W. G. Tisch, and J. P. Marangos, "High-order harmonic generation in graphite plasma plumes using ultrashort laser pulses: a systematic analysis of harmonic radiation and plasma conditions," J. Phys. B **45**(16), 165402 (2012).